NONLINEAR DYNAMIC MODELING OF ACTION POTENTIAL ENCODING IN TWO TYPES OF SPIDER MECHANORECEPTORS

Georgios D. Mitsis*, Andrew S. French**, Ulli Höger**, Spiros Courellis* and Vasilis Z. Marmarelis*

* Department of Biomedical Engineering, University of Southern California, Los Angeles CA, United States
** Department of Physiology and Biophysics, Dalhousie University, Halifax, NS, Canada

gmitsis@bmsr.usc.edu

Abstract: The encoding of mechanical stimuli into action potentials in two types of spider mechanoreceptor neurons is modeled by use of the principal dynamic modes (PDM) methodology. The PDM model is equivalent to the general Wiener-Bose model and consists of a minimum set of linear dynamic filters (PDMs), followed by a multivariate static nonlinearity and a threshold function. The PDMs are obtained by utilizing measurements of pseudorandom mechanical stimulation and the resulting action potentials. The static nonlinearity is computed as the locus of points of the latter that correspond to output action potentials. The performance of the model is assessed by computing receiver operating characteristic (ROC) curves and quantified by computing the area under the ROC curve. Three PDMs are revealed by the analysis. The first PDM exhibits a high-pass characteristic, illustrating the importance of the velocity of slit displacement in the generation of action potentials at the mechanoreceptor output, while the second and third PDMs exhibit band-pass and low-pass characteristics respectively. Differences between the Type A and B neurons are observed in the zeroth-order Volterra kernels as well as in the magnitudes of the second and third PDMs that perform band-pass and low-pass processing of the input signal respectively.

Introduction

Mechanoreceptors perform the detection and transduction of mechanical stimuli in many types of animal tissue, providing many inputs to the central nervous system. In addition to sensory functions, such as hearing, touch and balance, mechanoreceptors are involved in regulatory mechanisms in the cardiovascular, respiratory and renal systems. In order to accommodate a broad range of naturally occurring stimuli, mechanoreceptors are characterized by adaptive properties with respect to gain and operating range and they can subsequently exhibit a wide range of firing patterns.

The extraction of mathematical models that can accurately predict the responses of mechanoreceptors to a wide range of physiological stimuli can lead to a better understanding of the underlying physiology and the way in which the central nervous system receives information from internal and external mechanical events. However, the dynamic behavior of mechanoreceptors is not yet fully understood due to their small physical size and limited accessibility, as well as their complex and nonlinear characteristics. In previous modeling studies of mechanoreceptor function, linear techniques such as transfer function analysis have been employed as well as nonlinear Volterra-Wiener models have been utilized to describe the function of mechanoreceptors [1]-[3].

In the present study we model the dynamic transduction of mechanical stimuli into action potentials in two types of mechanoreceptor neurons from a spider lyriform organ that are morphologically similar but exhibit different dynamic characteristics. Type A neurons are rapidly adapting and produce only one or two action potentials in response to step electrical or mechanical stimuli, while Type B neurons adapt more slowly and produce a burst of many action potentials with similar stimuli.

For this purpose, we employ the principal dynamic mode (PDM) methodology for spike-output systems [4]. The PDM method aims to extract the most significant dynamic components of a nonlinear system in the form of a minimum set of linear filters that process the input, after estimating its first and second-order Volterra kernels [4]. The PDM outputs feed a multiple-input static nonlinearity and a subsequent threshold function to yield the output action potentials. This study extends our previous findings employing the PDM methodology to model the dynamics of the conversion of mechanical displacements into transmembrane receptor current and potential in a spider mechanoreceptor [5].

Materials and Methods

Animal protocols were approved by the Dalhousie University Committee on Laboratory Animals. Adult spiders, *Cupiennius salei*, of either sex were taken from a laboratory colony. A concave piece of cuticle containing the intact VS-3 lyriform organ, was dissected from the patella of an autotomized leg and mounted on a custom designed holder. The discontinuous (switching) single electrode current-clamp technique was used to

ISSN: 1727-1983

record cell membrane potentials with a SEC-10L amplifier (NPI Electronic, Tamm, Germany). For mechanical stimulation, a piezoelectric stimulator with position control feedback (LVPZ translator, PZT controller; Polytec Physik-Instrumente, Waldbronn, Germany) was mounted on a 3-dimensional micromanipulator that could position the tip of the stimulator probe beneath the outer surface of the VS-3 slits.

Pseudorandom Gaussian white noise was generated by a digital computer. Mechanical displacement was sensed by the position transducer in the piezoelectric stimulator, which had a low-pass characteristics with a corner frequency of ~80 Hz. Membrane potentials, including action potentials, were recorded from the amplifier. The duration of each recording was approximately 80 seconds.

Action potentials were separated from the underlying continuous membrane potentials and were digitally filtered by convolution with the sin(x)/x function to band-limit them to the range 0-500 Hz and produce a regularly sampled (1 ms interval) signal. Sampled analog signals of mechanical displacement were digitally re-sampled by averaging to give a 1 ms sample interval.

The PDM model of action potential encoding is shown in Fig. 1 and is equivalent to the Wiener-Bose model with a minimal set of linear filters $\{L_1, L_2, ..., L_m\}$. The discrete-time input signal $x(n)$ is convolved with the latter and the outputs are then fed into a multiple-input static nonlinearity, the output of which is compared to a threshold p to yield the model output.

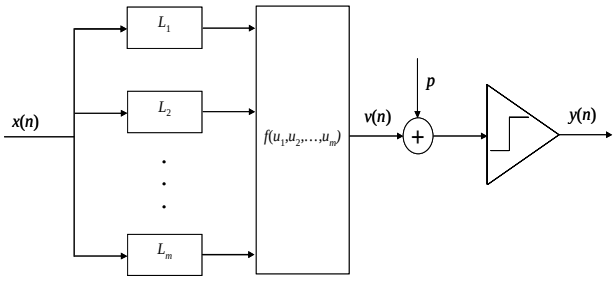

Figure 1: Principal Dynamic Mode (PDM) model of action potential firing in a spider mechanoreceptor

The PDM methodology [4] aims at extracting a minimum set of linear filters that remain functionally equivalent to the Wiener-Bose model, which constitute the PDMs of the system. This leads to compact representations that facilitate model interpretation, which is important in the case of physiological systems, as in the present study. The PDMs can be extracted from the estimates of the Volterra kernels of the system, as indicated below. The general discrete-time Volterra model for a finite-memory, Q-th order nonlinear system is:

$$y(n) = \sum_{q=0}^{Q} \left\{ \sum_{m_1} ... \sum_{m_q} k_q(m_1,..,m_q) x(n-m_1)...x(n-m_q) \right\} \quad (1)$$

where $k_q(m_1,..,m_q)$ are the linear (q=1) and nonlinear (q>1) Volterra kernels of the system, which describe the linear and nonlinear dynamic effects of the input on the output respectively. A practical way to estimate the kernels by employing stimulus-response data (in our case, mechanical displacements and the resulting action potentials) data is the Laguerre expansion technique [6], which expands the kernels in terms of the discrete-time Laguerre orthonormal basis and uses least-squares fitting to estimate the expansion coefficients. One way to estimate the PDMs from the first and second-order kernel estimates is to construct the matrix [4]:

$$\mathbf{R} = \begin{bmatrix} k_0 & \frac{1}{2}\mathbf{k}_1^{\mathrm{T}} \\ \frac{1}{2}\mathbf{k}_1 & \mathbf{k}_2 \end{bmatrix} \quad (2)$$

where k_0, $\mathbf{k_1}$, $\mathbf{k_2}$ are the zeroth, first and second-order Volterra kernels respectively. $\mathbf{R}$ is real symmetric, therefore its eigenvalues are always real. By selecting the most important eigenvalues λ_i of $\mathbf{R}$ on the basis of their magnitude, the corresponding orthonormal eigenvectors $\boldsymbol{\mu}_i$ define the PDMs of the system, i.e., the impulse responses of the linear filters of Fig. 1 [4]. The number of significant eigenvalues determines the number of the PDMs sufficient to describe the system dynamics.

The multivariate static nonlinearity $f(u_1,u_2,...,u_m)$ is defined as the locus of points that correspond to output action potentials. Therefore, f was constructed by first convolving the input with the PDMs, separating the space of the PDM outputs $(u_1,u_2,...,u_m)$ into m-dimensional bins, counting the number of points corresponding to output action potentials and dividing this number by the total number of points within each bin. Thus, $f(u_1,u_2,...,u_m)$ yields a measure of the probability of action potential firing as a function of the PDM outputs.

The PDM model performance in terms of predicting output action potentials correctly is assessed by constructing receiver operating characteristic (ROC) curves. In our case, ROC curves are plots of the true positive fraction as a function of the false positive fraction achieved by the PDM model for all output threshold p values between 0 and 1. Therefore, it was constructed by computing the binary output predicted by the PDM model for all values of threshold p between 0 to 1, counting the number of true and false positives and comparing the number and location of the predicted action potentials to those of their true counterparts. Finally, as a measure of the model performance, we computed the area under the ROC curve, which lies between 0 and 1. Area values that are closer to 1 denote better performance.

Of the approximately 80000 data points (sampled at 1 KHz) that were available for each of the four different neurons, segments of 5000 points were used to estimate the Volterra kernels and PDMs of the system. The

ISSN: 1727-1983

remaining data points were employed to construct the static nonlinearity by mapping the PDM output values onto the output action potentials (35000 points) and for model validation (35000 points).

Results

Data from four neurons (2 Type A and 2 Type B) were used for the analysis. Eigendecomposition of the matrix **R** given by Eq. (5) revealed three significant eigenvalues, the corresponding eigenvectors of which yielded the three PDMs $\boldsymbol{\mu}_1$, $\boldsymbol{\mu}_2$ and $\boldsymbol{\mu}_3$. Type B neurons were characterized by larger eigenvalue magnitudes. Representative PDMs are shown in Fig. 2 in the time and frequency domains for the one Type A and one Type B neuron, after scaling by the square root of the corresponding eigenvalue. The first (most significant) PDM has a high-pass (differentiating) characteristic, suggesting that its output depends primarily on the slit displacement velocity and secondarily on the displacement magnitude. The second PDM has a band-pass characteristic with a peak at around 180 Hz and a high-frequency plateau, implying dependence on the magnitude of slit displacement (position) in addition to the resonant behavior around 180 Hz. The third PDM has a low-pass characteristic that implies dependence only on the integrated (cumulative) slit displacement/position over a 6 ms time-window. The magnitude of the first PDM is similar between the two neuron types (with the type B neuron exhibiting a greater initial slope below 180 Hz), but the magnitude of the other two PDMs tended to be larger for the Type B neurons.

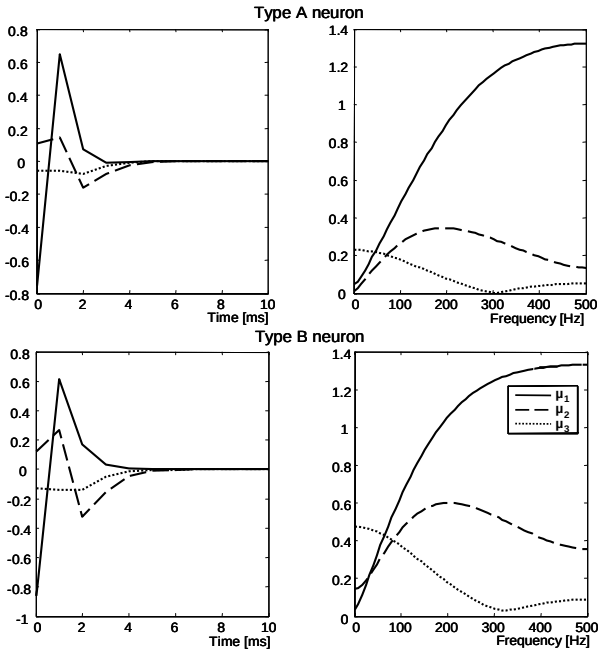

Figure 2: Representative PDMs, scaled by the square root of the corresponding eigenvalue for one Type A and one Type B neuron in the time and frequency domains.

In order to illustrate the combinations of PDM output values that gave rise to action potentials at the mechanoreceptor output, we show three-dimensional scatter plots of the PDM output values that corresponded to action potentials (blue) along with those that did not (red) for the Type A and Type B neurons in Fig. 3 and 4 respectively, as well as their corresponding two-dimensional projections on the $\{u_1, u_2\}$ planes in Fig. 5. The construction of the three-input nonlinear function $f(u_1, u_2, u_3)$ was based on these scatterograms through three-dimensional histograming that yielded the "Probability of Firing Function" (PFF) for each neuron. The form of the scatterograms and their projections indicates that both neuron types exhibit directionality with respect to the PDM output values (e.g., output action potentials corresponded to both positive and negative values of u_1, u_3, but almost all the output action potentials corresponded to negative values of u_2).

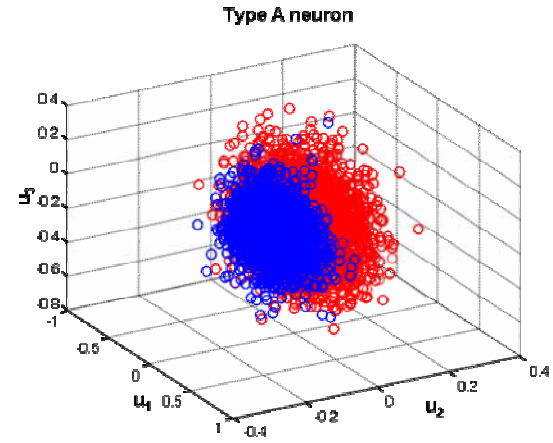

Figure 3: Scatter plot of the PDM output values that correspond to action potentials (blue) for a Type A neuron.

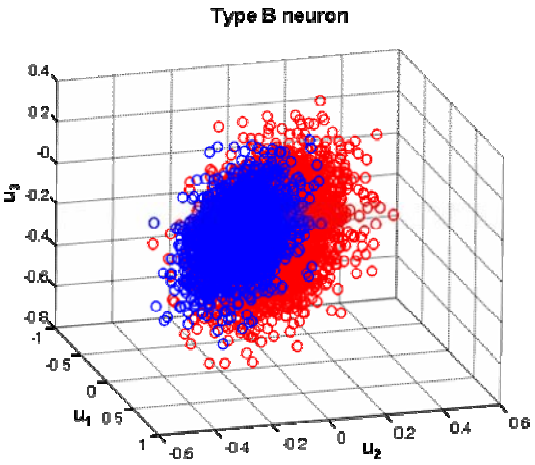

Figure 4: Scatter plot of the three PDM output values that correspond to action potentials (blue) for a Type B neuron.

ISSN: 1727-1983

Since $f(u_1,u_2,u_3)$ is three-dimensional, we plot its two-dimensional projection (marginal probability) on the $\{u_1,u_2\}$ planes, $f_M(u_1,u_2)$ in Fig. 5. Its form is similar for the Type A and Type B neurons, in agreement to the observations made for the scatterograms. The two-dimensional projection is symmetric with respect to the magnitude of u_1 around zero, suggesting that $f_M(u_1,u_2)$ depends on the magnitude of the slit displacement velocity but not on its direction. On the other hand, it is asymmetric with respect to u_2, yielding significant values for negative u_2 values only and implying directional dependence on the second PDM output. Overall, the asymmetric behavior was more pronounced for the output of the band-pass PDM u_2.

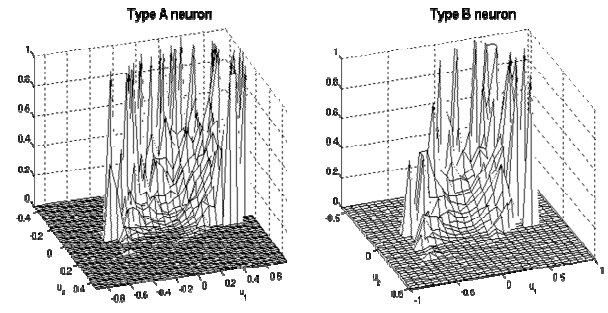

Figure 5: Projection of the three-dimensional static nonlinearity $f(u_1,u_2,u_3)$ on the $\{u_1,u_2\}$ plane (marginal probability function) for one Type A and one Type B neuron.

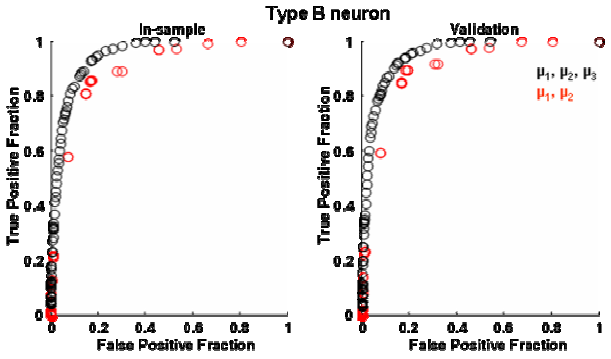

Figure 6: ROC curves for a Type B neuron for two (red) and three (black) PDM models.

Table 1: Area under the ROC curve for output action potential prediction, Type A and B neurons.

	Type A		Type B	
	Neuron 1	Neuron 2	Neuron 1	Neuron 2
Linear	0.989	0.953	0.919	0.956
μ_1, μ_2	0.988	0.936	0.938	0.958
μ_1, μ_2, μ_3	0.989	0.969	0.960	0.965

The ROC curves for the in-sample data (i.e., the points that were used to compute the PFF) and for the validation (out-of-sample) data for a Type B neuron are shown in Fig. 6 for a histogramming bin size of 0.1. The ROC curves for the rest of the neurons were found to be similar to those of Fig. 6. When three PDMs were utilized (black), i.e., a three-dimensional PFF was constructed, the performance improved considerably compared to two PDMs (red), which yielded a two-dimensional PFF. The ROC curve is a suitable measure of model performance in terms of predicting output action potentials, since it yields an overall assessment of performance for all values of the threshold *p*, which can be quantified by calculating the area under the curve. The values of the area under the ROC curves of Fig. 6 were equal to 0.930/0.957 (in-sample data) and 0.938/0.960 (validation data) for two/three PDMs respectively. The model performance for the validation data set is thus comparable to its in-sample counterpart, corroborating the validity of the modeling results.

The corresponding values for the validation data sets for all four neurons are given in Table 1 for a histogramming bin size of 0.1. For smaller bin sizes (i.e., finer resolution in the PFF computation), the performance improved for the in-sample data but degraded considerably for the validation data. This is to be expected, since the number of data points corresponding to action potentials was low compared to the total number of data points. The best overall performance for both in-sample and validation data was observed for a bin size of 0.1. For comparison purposes, the values of the area under the ROC curve achieved by linear Volterra models are also given. Interestingly, nonlinear models improve the performance marginally for one Type A neuron, while this improvement is substantial for all other neurons, especially for the two Type B neurons. This suggests that the nonlinear component is stronger in the latter.

Discussion

The dynamics of the two neuron types were generally similar, although some differences were observed in the magnitude of the second (band-pass) and third (low-pass) PDMs, which were found to be larger for Type B neurons. Differences were also observed in the frequency-domain slope of the first (high-pass) PDM below 180 Hz, which may be significant for the overall response characteristics of the neuron, since most of the mechanical stimulus power was below 180 Hz. The constant component of the model (zeroth-order kernel), which is related to the average firing rate, was also found to be considerably larger for Type B neurons. These observations extend our previous modeling studies of the transduction of mechanical stimuli into intracellular receptor current and voltage [5].

Nonlinear models were found to improve the model performance considerably, when compared to linear models, in terms of both prediction NMSE (10-15% reduction) and area under the ROC curve (Table 1). Third-order Volterra models further improved the output prediction of second-order models, resulting in about 5% reduction of the prediction NMSE (from around 80% to 75%). However, second and third-order

ISSN: 1727-1983

models yielded comparable ROC curve area values. This may be attributed to the fact that third-order models built mainly on the contribution of second-order models to both true and false positive spikes, without altering significantly the relation between true and false positives. The improvement observed for nonlinear models was more pronounced for Type B neurons, implying a stronger nonlinear component in the dynamics of the latter. The presence of third-order nonlinearities in the mechanoreceptor function is also suggested by the form of the calculated PFFs, which exhibited half-wave rectification characteristics.

The characteristics of the three PDMs suggest that both Type A and B neurons are able to encode more than one parameter of the slit displacement stimulus (i.e., velocity, position and cumulative position). The first PDM, which resembled the first-order Volterra kernel, had a differentiating (high-pass) characteristic and encoded primarily the stimulus velocity – although some position encoding also took place by virtue of the fact that the positive and negative peak deflections of the PDM in the time domain were not equal (they would be equal in case of a strictly differentiating PDM). The second and third PDMs had mixed band-pass and low-pass characteristics, implying encoding of velocity (within a preferred range defined by the pass-band), position and cumulative position.

The scatterograms of Figs. 3-4 show that the mapping between the PDM output values and the resulting action potentials was similar in Type A and B neurons, which is also reflected in the PFFs of Fig. 5. The latter suggest that action potential encoding was directionally selective mostly with respect to the preferred-velocity and position of the displacement, since the marginal PFF $f_M(u_1,u_2)$ was nonzero for negative values of the second PDM output u_2 only (Fig. 5); whereas it was symmetric with respect to the primarily velocity-dependent PDM output u_1. The strong directional selectivity with respect to position was also observed for the transduction of mechanical stimuli into transmembrane current and potential [5].

The discrepancy observed between their estimated zeroth-order kernel values may reflect their differences in the recovery from Na^+ channel inactivation. Voltage-activated sodium current (I_{Na}) is primarily responsible for the leading edge of the action potential in many neurons. While I_{Na} generally activates rapidly when a neuron is depolarized, its inactivation properties vary significantly among different neurons and it can occasionally exhibit slowly and rapidly inactivating components within the same neuron. In the case of Type A and B neurons, it has been shown with voltage-clamp experiments [6] that the differences in their response characteristics are due primarily to the Na^+ channel inactivation properties and particularly the recovery from inactivation, which was found to be significantly slower in Type A neurons. The same was demonstrated by using a simplified Hodgkin-Huxley model [7], where the firing patterns of Type A and B neurons were reproduced by using different time constants for the I_{Na} recovery from inactivation (120 ms and 40 ms respectively), as well as different slope factors (5 mV and 9 mV respectively). However, the fast I_{Na} activation and inactivation dynamics, which have been shown to be similar in Type A and B neurons with single time constants of 2-3 ms and 5-10 ms respectively [7], may dominate the obtained estimates in the present study (the kernel memory was found to be about 10-15 ms). Therefore, we postulate that the different characteristics of the I_{Na} recovery from inactivation are reflected mainly on the zeroth-order model component. We must also note that pseudorandom stimulation results in continuous action potential firing, therefore Na^+ channels may not be inactivated or recover from inactivation completely, as in the case of step stimulation used in the aforementioned studies.

Conclusions

The PDM analysis provides a compact representation of mechanoreceptor dynamics, which describes quantitatively their ability to encode multiple features of mechanical stimuli and achieves excellent performance in terms of predicting the resulting action potentials. It can also assist in understanding and dissecting the underlying physiological mechanisms, when combined with suitable experimental manipulation of the relevant ionic processes.

References

[1] FRENCH A.S., HÖGER U., SEKIZAWA S.I., AND TORKKELI P.H. (2001) "Frequency response functions and information capacities of paired mechanoreceptor neurons", *Biol. Cybern.*, **85**, pp. 293-300

[2] FRENCH A.S. AND MARMARELIS V.Z. (1995) "Nonlinear neuronal mode analysis of action potential encoding in the cockroach tactile spin neuron", *Biol. Cybern.*, **73**, pp 425-430

[3] GAMBLE E.R. AND DICAPRIO R.A. (2003) "Nonspiking and spiking proprioceptors in the crab: white noise analysis of spiking CB-chordotonal organ afferents", *J. Neurophysiol.*, **89**, pp. 1815-1825

[4] MARMARELIS V.Z. (1997) "Modeling methodology for nonlinear physiological systems", *Ann. Biomed. Eng.*, **25**, pp. 239-251

[5] MARMARELIS V.Z., JUUSOLA M., FRENCH A.S. (1999) "Principal dynamic mode analysis of nonlinear transduction in a spider mechanoreceptor", *Ann. Biomed. Eng.*, **27**, pp. 391-402

[6] TORKKELI P.H., SEKIZAWA S.I. AND FRENCH A.S. (2001) "Inactivation of voltage-activated Na^+ currents contributes to different adaptation properties of paired mechanosensory neurons", *J. Neurophysiol.*, **85**, pp. 1595–1602

[7] TORKKELI P.H. AND FRENCH A.S. (2002) "Simulation of different firing patterns in paired spider mechanoreceptor neurons: The role of Na^+ channel inactivation", *J. Neurophysiol.*, **87**, pp. 1363-1368

ISSN: 1727-1983